iScience

Article

Dual opposing quadrature-PT symmetry

Graphical abstract

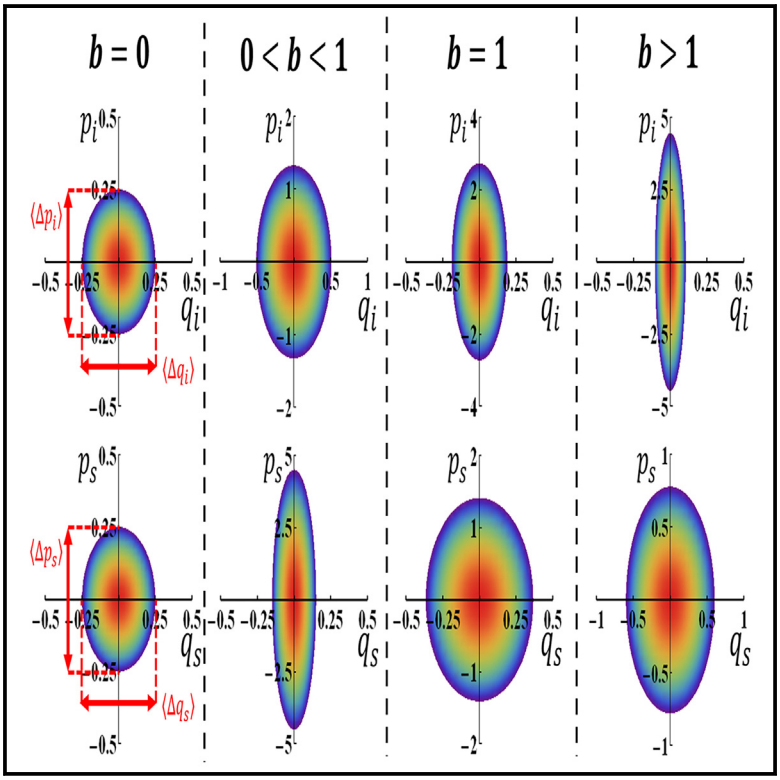

Highlights

- This is an optimal quantum platform for investigating dual opposing quadrature-PT symmetry
- This work establishes a link between PT symmetry, nonclassicality, and the EPR paradox
- Our findings unveil nontrivial quantum aspects of PT symmetry

Authors

Wencong Wang, Jacob Kokinda, Jiazhen Li, Qing Gu, Dongmei Liu, Jianming Wen

Correspondence

dmliu@scnu.edu.cn (D.L.), jwen7@binghamton.edu (J.W.)

In brief

Natural sciences; Physics; Quantum physics

Wang et al., 2025, iScience *28*, 111655
January 17, 2025
https://doi.org/10.1016/j.isci.2024.111655

CellPress

iScience

CellPress
OPEN ACCESS

Article

Dual opposing quadrature-PT symmetry

Wencong Wang,[1] Jacob Kokinda,[2] Jiazhen Li,[2] Qing Gu,[2,3] Dongmei Liu,[1,*] and Jianming Wen[4,5,*]
[1]Guangdong Provincial Key Laboratory of Quantum Engineering and Quantum Materials, School of Physics and Telecommunication Engineering, South China Normal University, Guangzhou 510006, China
[2]Department of Electrical and Computer Engineering, North Carolina State University, Raleigh, NC 27695, USA
[3]Department of Physics, North Carolina State University, Raleigh, NC 27695, USA
[4]Department of Electrical and Computering Engineering, Binghamton University, Binghamton, NY 13902, USA
[5]Lead contact
*Correspondence: dmliu@scnu.edu.cn (D.L.), jwen7@binghamton.edu (J.W.)
https://doi.org/10.1016/j.isci.2024.111655

SUMMARY

Our recent research on type-I quadrature parity-time (PT) symmetry, utilizing an open twin-beam system, not only enables observing genuine quantum photonic PT symmetry amid phase-sensitive amplification (PSA) and loss in the presence of Langevin noise but also reveals an additional classical-to-quantum (C2Q) transition in noise fluctuations. In contrast to the previous setup, our exploration of an alternative system assuming no loss involves a type-II PSA-only scheme. This scheme facilitates dual opposing quadrature-PT symmetry, offering a comprehensive and complementary comprehension of C2Q transitions and PT-enhanced quantum sensing with optimal performance in the symmetry unbroken region. Furthermore, our investigation into the quantum correlation with the Einstein-Podolsky-Rosen criteria uncovers previously unexplored connections between PT symmetry and nonclassicality, as well as quantum entanglement within the continuous-variable framework.

INTRODUCTION

Over the past decade, classical linear and nonlinear photonic systems, characterized by gain and loss, have served as a robust and versatile platform for exploring non-Hermitian (NH) physics. Notably, these systems have played a key role in probing parity-time (PT) symmetry,[1–17] unveiling a variety of peculiar effects absent in Hermitian counterparts. These effects include the typical PT phase transition, where eigenvalues transition from real to imaginary, and the coalescence of eigenvalues and eigenvectors at the phase transition point, known as the exceptional point (EP). The significant achievements in classical PT systems have prompted a recent shift in focus toward open quantum optical systems[18–25] with an aim to disclose distinctive quantum features.

However, challenges[26,27] like Langevin noise, the quantum noncloning theorem, and the causality principle have led to the prevailing belief that quantum optical PT symmetry with both gain and loss is unlikely. This limitation confines research mainly to dissipative single-partite systems, such as single photons,[18,22] ultracold atoms,[21] trapped ions,[19,23] nitrogen-vacancy centers[20] in diamond, and superconducting qubits[24]–utilizing postselection measurement. Consequently, observed PT phase transitions closely resemble classical NH scenarios, rooted in a (semi)classical interpretation. Unfortunately, these studies fail to offer insights on the viability of gain-loss-coupled quantum optical PT symmetry or unique effects exclusive to quantum NH settings absent in classical NH or Hermitian quantum counterparts.

Unlike prior research, our recent work[28] demonstrates the attainability of genuine quantum optical PT symmetry in an open twin-beam system through four-wave mixing (FWM), overcoming these challenges by employing phase-sensitive amplification (PSA) instead of phase-insensitive amplification (PIA) and studying field quadrature observables. Remarkably, under fair sampling measurement, our PSA-loss bipartite system establishes unique type-I quadrature-PT symmetry without a classical analog, introducing an additional dynamical or stationary classical-to-quantum (C2Q) transition in quadrature noise fluctuations alongside the standard PT phase transition in eigenvalues. The emergence of these dual transitions in the continuous-variable (CV) framework is a minimum signature for claiming quantum behavior, as further supported by our recent studies[29,30] on a dissipative spin-boson-coupled superconducting circuit platform, showcasing the co-emergence of eigenspectral phase transition and exceptional entanglement transition in the Fock space through post-projection measure.

In our previous vacuum-input type-I quadrature-PT configuration,[28] the system displays unconventional features challenging conventional expectations of quantum squeezing. Notably, there is no need for a cavity or high parametric gain, and the system exhibits anomalous loss-induced quadrature squeezing. Moreover, although the quadrature-PT behaviors manifest various sharp C2Q transitions related to quadrature noise fluctuations, the EP generally does not coincide with these C2Q transition boundaries. Furthermore, the nontrivial interference between PSA or loss and parametric conversion expedites the emergence of nonclassical correlations beyond traditional quantum

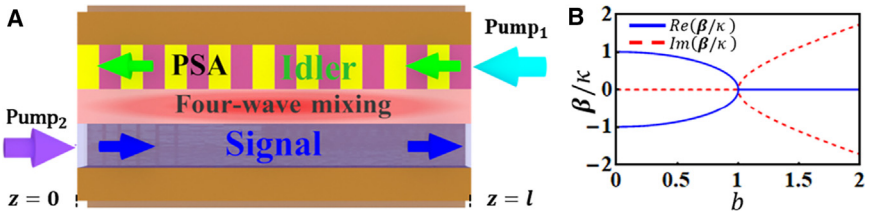

Figure 1. Schematic diagram of the theoretical model

(A) Dual opposing type-II quadrature-PT symmetry emerges in twin-beam generation, with the backward-propagating idler mode undergoing PSA at a rate of g, whereas the forward-propagating signal experiences lossless transmission.
(B) Regular PT phase transition associated with eigenvalues $\pm\beta$.

squeezing, necessitating additional conditions. Here, we deepen our understanding of quadrature-PT symmetry and its effects on the twin-beam system by considering no loss and only involving PSA (Figure 1A). Differing from the previous PSA-loss (type-I) case, both quadrature pairs in this type-II PSA-only scheme evolve with contrasting PT symmetry, resulting in dual opposing quadrature-PT symmetry. Additionally, this type-II system emerges as a quintessential platform to unveil various intriguing physics including its profound connection with the renowned Einstein-Podolsky-Rosen (EPR) correlations, a territory largely uncharted in NH settings thus far.

RESULTS

Theoretical model

Assuming undepleted and classical input pump lasers, the evolution of correlated signal-idler field operators a_s and a_i along the $\pm z$-direction is governed by the Hamiltonian $H = i\hbar g(a_i^2 - a_i^{\dagger 2})/2 + \hbar\kappa(a_i^\dagger a_s^\dagger + a_i a_s)$. The corresponding Heisenberg equations are $da_i/dz = ga_i^\dagger + i\kappa a_s^\dagger$ and $da_s/dz = -i\kappa a_i^\dagger$, where $\dagger, g, \kappa$ denote the Hermitian conjugate, PSA, and FWM parametric conversion coefficient, respectively. Akin to our latest work,[28] hidden PT symmetry emerges upon transforming them into coupled-quadrature forms,

$$\frac{d}{dz}\begin{bmatrix} q_i \\ p_s \end{bmatrix} = \begin{bmatrix} g & \kappa \\ -\kappa & 0 \end{bmatrix}\begin{bmatrix} q_i \\ p_s \end{bmatrix}, \quad \text{(Equation 1)}$$

$$\frac{d}{dz}\begin{bmatrix} p_i \\ q_s \end{bmatrix} = \begin{bmatrix} -g & \kappa \\ -\kappa & 0 \end{bmatrix}\begin{bmatrix} p_i \\ q_s \end{bmatrix}, \quad \text{(Equation 2)}$$

by introducing $q_j = (a_j^\dagger + a_j)/2$ and $p_j = i(a_j^\dagger - a_j)/2$ $(j = i, s)$ with the commutation relation $[q_j, p_j] = i/2$. As detailed in the Supplementary Information (SI), the quadrature pair $\{q_i, p_s\}$ follows active PT symmetry, whereas the other pair $\{p_i, q_s\}$ obeys passive PT symmetry after opposite gauge transformations. Both pairs share the same EP at $b = g/2\kappa = 1$, with an identical pair of eigen-propagation values $\pm\beta = \pm\kappa\sqrt{1 - b^2}$ phase transitioning from real to imaginary for $b < 1$ and $b > 1$. This striking phenomenon, termed *dual opposing quadrature-PT symmetry*, represents a pure quantum effect that is inaccessible in PIA-based structures. For a medium of length l, the solutions of Equations 1 and 2 are

$$\begin{bmatrix} q_i(0) \\ p_s(l) \end{bmatrix} = \frac{-\sin\epsilon}{\sin(\beta l + \epsilon)}\begin{bmatrix} -e^{-\frac{gl}{2}} & \frac{\sin(\beta l)}{\sin\epsilon} \\ \frac{\sin(\beta l)}{\sin\epsilon} & -e^{\frac{gl}{2}} \end{bmatrix}\begin{bmatrix} q_i(l) \\ p_s(0) \end{bmatrix}, \quad \text{(Equation 3)}$$

$$\begin{bmatrix} q_s(l) \\ p_i(0) \end{bmatrix} = \frac{\sin\epsilon}{\sin(\beta l - \epsilon)}\begin{bmatrix} -e^{-\frac{gl}{2}} & \frac{\sin(\beta l)}{\sin\epsilon} \\ \frac{\sin(\beta l)}{\sin\epsilon} & -e^{\frac{gl}{2}} \end{bmatrix}\begin{bmatrix} q_s(0) \\ p_i(l) \end{bmatrix}, \quad \text{(Equation 4)}$$

where $\epsilon = \tan^{-1}(2\beta/g)$ is a PT-induced phase shift. Their physics significance will become clear shortly.

Homodyne detection

The concise and symmetrical structures of Equations 3 and 4 render them well-suited and mutually complementary for probing the fundamental nature of dual opposing quadrature-PT symmetry. They offer valuable insights into physical phenomena, including versatile C2Q transitions, and effectively address causality concerns, particularly in single-mode quadrature scenarios. We thus focus on four single-mode quadrature variances, $\langle\Delta q_j^2\rangle = \langle q_j^2\rangle - \langle q_j\rangle^2$ and $\langle\Delta p_j^2\rangle = \langle p_j^2\rangle - \langle p_j\rangle^2$, leaving the two-mode quadrature and relative-intensity squeezing cases for the SI. Applying Equations 3 and 4, we arrive at exact expressions for these four variances,

$$\langle\Delta q_i^2(0)\rangle = \frac{e^{-gl}\sin^2\epsilon + \sin^2(\beta l)}{4\sin^2(\beta l + \epsilon)}, \quad \text{(Equation 5)}$$

$$\langle\Delta p_s^2(l)\rangle = \frac{e^{gl}\sin^2\epsilon + \sin^2(\beta l)}{4\sin^2(\beta l + \epsilon)}, \quad \text{(Equation 6)}$$

$$\langle\Delta q_s^2(l)\rangle = \frac{e^{-gl}\sin^2\epsilon + \sin^2(\beta l)}{4\sin^2(\beta l - \epsilon)}, \quad \text{(Equation 7)}$$

$$\langle\Delta p_i^2(0)\rangle = \frac{e^{gl}\sin^2\epsilon + \sin^2(\beta l)}{4\sin^2(\beta l - \epsilon)}, \quad \text{(Equation 8)}$$

where Equations 5 and 6 are mathematically symmetric to Equations 7 and 8. For active PT-symmetric $\{q_i(0), p_s(l)\}$, superluminal (fast) light effects are expected, indicated by an advanced phase shift $+\epsilon$ in the variances. Conversely, passive PT-symmetric $\{q_s(l), p_i(0)\}$ are anticipated to manifest subluminal (slow) light effects, evident in a phase delay $-\epsilon$ in their variances. Causality is maintained despite potential effects, as individual signal or idler fields exist in mixed states. In the presence of optical loss,[28] Langevin noise obscures the observation of slow- and fast-light effects, making it challenging to detect

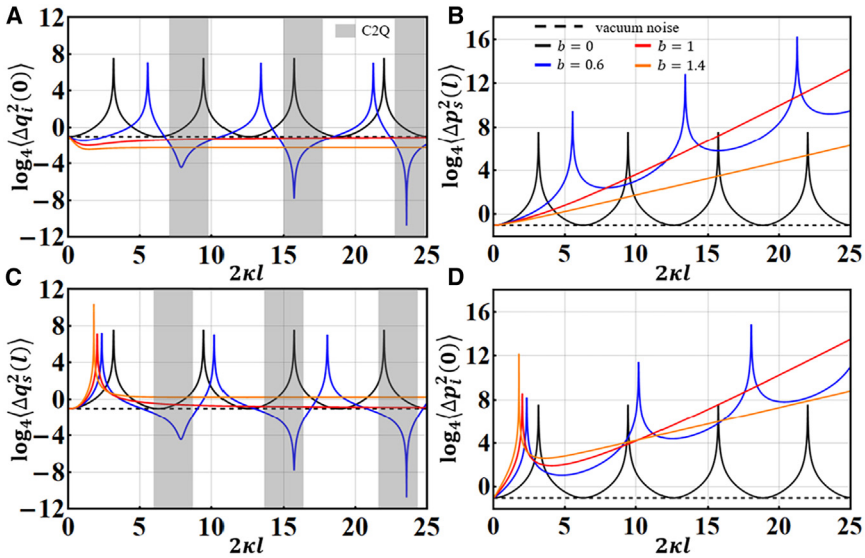

Figure 2. Single-mode variance in homodyne detection

Compared with standard TMSV ($b = 0$, black solid line) and vacuum noise (black dashed line), the quadrature variances $\{\langle\Delta q_i^2(0)\rangle, \langle\Delta p_s^2(l)\rangle\}$ (A and B) and $\{\langle\Delta q_s^2(l)\rangle, \langle\Delta p_i^2(0)\rangle\}$ (C and D) feature active and passive PT-induced quadrature squeezing and de-squeezing, respectively. In the PT phase-unbroken region ($b<1$), $\langle\Delta q_i^2(0)\rangle$ and $\langle\Delta q_s^2(l)\rangle$ concurrently display flexible-length dynamical C2Q transitions, whereas complementary stationary C2Q transitions occur for a fixed length (shaded gray areas) with the EP-variance curves serving as the exact boundary between the incompatible classical and quantum noise realms.

them in the type-I scenario. Besides, PT symmetry disrupts symmetric noise characteristics and 2π-periodicity in usual two-mode squeezed vacuum (TMSV), facilitating the rapid emergence of quantum squeezing and exceptional C2Q transitions. The implications of these results are apparent in the numerical plots against the dimensionless propagation variable $2\kappa l$ for various b during $\pm\beta$-phase transitions (Figures 2A–2D). Under the same κ, the ideal TMSV ($g = 0$, solid black curves) fails to yield quantum squeezing, with each quadrature variance oscillating above the vacuum noise (dashed black lines).

For active quadrature-PT symmetry in its phase-unbroken region ($b<1$), logarithmic $\langle\Delta q_i^2(0)\rangle$ (Figure 2A) periodically fluctuates at a new period $T = 2\pi\kappa/\beta$. Gradually growing squeezing peaks at trough locations nT (with n as positive integers), even without a cavity, signifying flexible-length dynamical C2Q transitions with other fixed parameters. In the phase-broken regime ($b>1$), periodic noise distributions cease, and quantum noise reduction remains consistently available. A larger b results in greater quantum squeezing. Importantly, the variance curve at the EP serves as the partition line, distinguishing these two distinct noise behaviors. Note that the stationary C2Q transition (shaded gray areas) can also occur at a fixed length by changing only g, where the EP-variance again acts as the exact boundary dividing the incompatible classical and quantum noise worlds. Contrastingly, logarithmic $\langle\Delta p_s^2(l)\rangle$ (Figure 2B) assumes similar periodic classical fluctuations peaking at $(nT - 2\epsilon\kappa/\beta)$ for the intact PT phase. As symmetry spontaneously breaks down, it grows monotonically with an upper bound set by the EP-variance, and the greater the b value, the less the de-squeezing.

For passive quadrature-PT, $\langle\Delta q_s^2(l)\rangle$ and $\langle\Delta p_i^2(0)\rangle$ (Figures 2C and 2D) behave similarly despite with distinct patterns. Specifically, when $b<1$, $\langle\Delta q_s^2(l)\rangle$ shows noticeable quadrature squeezing, akin to $\langle\Delta q_i^2(0)\rangle$, but with periodic squeezing amplitudes shifting to $[(n-1)T + 2\epsilon\kappa/\beta]$, implying flexible-length dynamical C2Q transitions. In contrast, $\langle\Delta p_i^2(0)\rangle$ amplifies classical noise with periodic fluctuations, similar to $\langle\Delta p_s^2(l)\rangle$. When $b \gtrless 1$, apart from a lone peak at $l = \epsilon/\beta$, $\langle\Delta q_s^2(l)\rangle$ is anti-squeezed, and increasing b intensifies the anti-squeezing. Compared to $\langle\Delta q_i^2(0)\rangle$, a complementary stationary C2Q transition at a fixed length (shaded gray areas) appears alongside the $\pm\beta$-based PT-phase transition by manipulating only g. For $\langle\Delta p_i^2(0)\rangle$, it exhibits classical noise amplification regardless of PT symmetry collapse, akin to $\langle\Delta p_s^2(l)\rangle$. The distinction between these variances is evident. The periodic fluctuations of $\langle\Delta p_i^2(0)\rangle$ (Figure 2D) precede those of $\langle\Delta p_s^2(l)\rangle$ by a net phase $2\kappa(2\epsilon - \pi)/\beta$ before the PT-phase breaks. After the phase breaks, $\langle\Delta p_i^2(0)\rangle$ always peaks around $l = \epsilon/\beta$ before growing monotonically. The separation distance between any two adjacent peaks (or valleys) is $(\pi - 2\epsilon)/\beta$, uniform for all four periodically fluctuating variances. Previous work[28] has documented that the presence of a balanced loss to the signal mode diminishes the symmetry of the entire system, inducing divergent courses in the two sets of conjugate quadrature pairs.

Nonclassicality and EPR correlation

Other than showing the dual transitions, this succinct system is an excellent toolbox for disclosing the singular relation between PT symmetry and nonclassicality, an emerging frontier barely touched to date. To delve into this, we first employ the EPR criteria proposed by Reid[31,32] to seek resolutions. We note that the four single-mode quadratures (2a) and (2b) coincide with their respective amplitudes and phases, namely, $X_1(0) = q_i(0), X_2(0) = p_i(0), Y_1(l) = q_s(l)$ and $Y_2(l) = p_s(l)$ (SI). Consequently, the Cauchy-Schwarz inequality for these quadrature phase amplitudes can be explored by examining the quantum-mechanical correlation coefficients,

$$|C_{jm}| = \left|\frac{\langle X_j(0)Y_m(l)\rangle}{\sqrt{\langle[X_j(0)]^2\rangle\langle[Y_m(l)]^2\rangle}}\right| \ngtr 1, \qquad \text{(Equation 9)}$$

with $\{j,m\} = \{1,2\}$. After some calculations (SI), we have

$$C_{jj} = 0, \qquad \text{(Equation 10)}$$

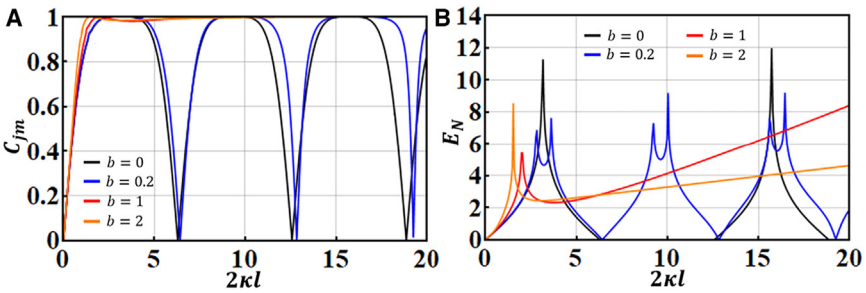

Figure 3. Entanglement properties

Assessing the impact of PT symmetry on nonclassicality using the quantum correlation coefficient C_{jm} (A) and logarithmic negativity E_N (B) in the PT-symmetry phase unbroken region (blue), at the exceptional point (red), and in the PT-symmetry phase broken region (orange), compared to the standard TMSV case (black curve with $b = 0$).

$$C_{jm} = \frac{2\cosh(gl/2)\sin\epsilon\sin(\beta l)}{\sqrt{\sin^4\epsilon+\sin^4(\beta l)+2\cosh(gl)\sin^2\epsilon\sin^2(\beta l)}}, \quad \text{(Equation 11)}$$

with $j \neq m$. Physically, $|C_{jm}| = 1$ means a state of perfect quantum correlation between $X_j(0)$ and $Y_m(l)$, whereas $|C_{jm}| = 0$ implies a complete absence of such correlation between the two.

Therefore, Equation 10 denotes a complete lack of nonclassical correlation between $X_1(0)$ $(X_2(0))$ and $Y_1(l)$ $(Y_2(l))$ regardless of the presence of PT symmetry. In contrast, the situation described by Equation 11 becomes subtle for the pair $\{X_1(0), Y_2(l)\}$ (or $\{X_2(0), Y_1(l)\}$). To see its behavior, (Figure 3A) numerically plots C_{12} (or C_{21}) with three representative examples, revealing abrupt changes made by PT symmetry. Prior to the phase breaking $(b < 1)$, $|C_{12}|$ or $|C_{21}|$ oscillates between 1 and 0 at the period $2\pi\kappa/\beta$ (blue curve with $b = 0.2$) but differs substantially from the conventional TMSV case ($g = 0$ or $b = 0$, black line), demonstrating periodic shifts between the perfect existence and complete absence of quantum correlation. Contrarily, after the phase transition $(b > 1)$, it asymptotically approaches unity (orange curve with $b = 2$), implying a perfect quantum correlation between the cross-quadrature phase amplitudes. Here, the EP-line (red curve with $b = 1$) simply acts as the circumscription to differentiate curve patterns across the PT phase transition. In essence, the scenario resembles the EPR *Gedankenexperiment*.[33] In the $b \ngeq 1$ region, maximum correlation between amplitude $X_1(0)$ and $Y_2(l)$, as well as between $X_2(0)$ and $Y_1(l)$, can be easily achieved, leading to the application of EPR reasoning. In the $b < 1$ regime, the EPR scenario applies broadly to these two quadrature phase amplitude pairs, although it may depend on the propagation distance. It is worth noting that the influence of anti-Hermiticity on EPR correlations here is analogous to the impact of non-Hermiticity on quantum entanglement in a dissipative spin-boson system, that is, PT symmetry gives rise to extra exceptional nonclassical phenomena.[29,30]

The extent of nonclassicality in the system can be further assessed through the analysis of logarithmic negativity,[34,35] denoted as $E_N = \max[0, -\ln 4\eta]$, derived from the system's 4 by 4 covariance matrix $V_Q = [A, C; C^{\mathrm{Tr}}, B]$ (see supplemental information). Here, $\eta = \sqrt{(\Sigma - \sqrt{\Sigma^2 - 4\det V_Q})/2}$ and $\Sigma = \det A + \det B - 2\det C$ with $A = [\langle\Delta q_i^2(0)\rangle, 0; 0, \langle\Delta p_i^2(0)\rangle]$, $B = [\langle\Delta q_s^2(l)\rangle, 0; 0, \langle\Delta p_s^2(l)\rangle]$, $C = [0, \langle q_i(0)p_s(l)\rangle - \langle q_i(0)\rangle\langle p_s(l)\rangle; \langle q_s(l)p_i(0)\rangle - \langle q_s(l)\rangle\langle p_i(0)\rangle, 0]$, and Tr representing transpose. The farther the quantum correlation that E_N reflects, the farther it is from 0. In (Figure 3B), we present representative examples both before and after the β-phase transition, comparing them with the TMSV case (black). For $b < 1$, E_N exhibits gradually increasing bimodal cyclical oscillations above zero, reaching zero only at valleys. This signifies a substantially enlarged range with quantum emergence. In contrast, for $b \ngeq 1$, E_N develops a single peak that is always larger than 0, indicating a full spectrum of quantum availability. As evident, the analysis of E_N aligns with the previously discussed analysis of C_{jm} $(j \neq k)$ except from the entire system perspective.

Quantum sensing

As a pivotal nonclassical resource, quantum squeezing[36] plays a key role in traditional quantum sensing and metrological applications.[37] Recent studies[38,39] leveraging anti-PT symmetry have demonstrated enhanced squeezing-based quantum sensitivity near EP. This prompts an exploration of whether improved sensitivity is attainable in our type-II quadrature-PT system. In contrast to the type-I quadrature-PT case,[28] the type-II system arises as a versatile PT-enhanced quantum sensor with unparalleled performance, surpassing designs based on squeezing factors or EP alone. Besides, passive PT quadrature outperforms active PT quadrature, and two-mode quadrature outshines single-mode quadrature (SI) under the same system parameters. The achievable precision approaches the quantum Cramér-Rao bound, dictated by the quantum Fisher information (QFI) of the quantum state, although it experiences a loss of sensitivity near and above the EP.

To commence, we assume the initial preparation of the two bosonic modes in a two-photon coherent state, $|\Phi\rangle_0 = |\alpha_i, \alpha_s\rangle$. Subsequently, we set $\alpha_i = i\alpha_s^* \equiv \sqrt{2}\alpha e^{i\pi/4}$ for simplification in the upcoming calculations. In the case of single-mode quadrature, homodyning detection is applied at an interaction distance l to an observable, say, $q_i(0)$. Utilizing Equation 3, we find the mean value and variance of $q_i(0)$ to be

$$\langle q_i(0)\rangle = \frac{e^{-\frac{gl}{2}}\sin\epsilon\langle q_i(l)\rangle - \sin(\beta l)\langle p_s(0)\rangle}{\sin(\beta l+\epsilon)}. \quad \text{(Equation 12)}$$

The ultimate accuracy of sensing relies on the precision with which a small change in $\langle q_i(0)\rangle$ can be measured in response

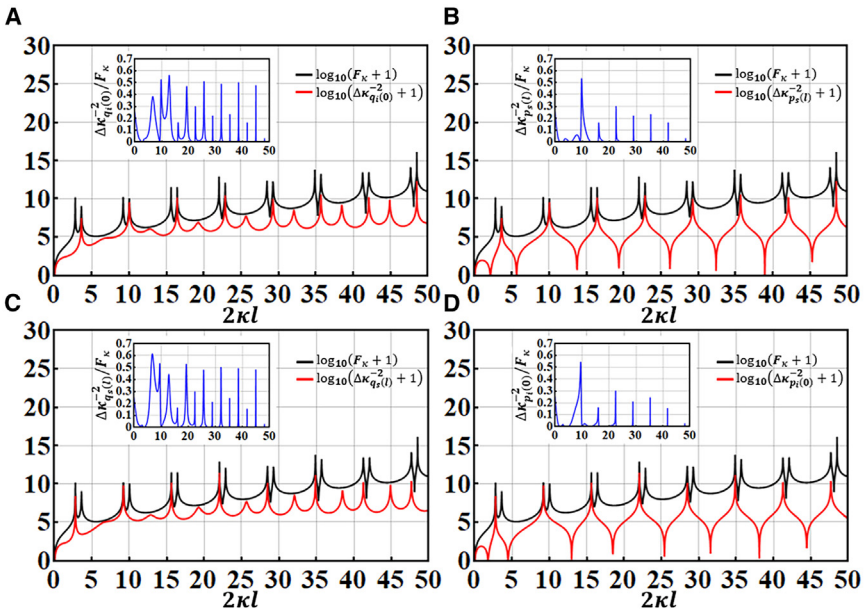

Figure 4. Quantum sensing performance

Quadrature-PT-symmetric quantum sensing. The ratios of the inverse variances $\log_{10}\left(\Delta\kappa^{-2}_{q_i(0)}+1\right)$ (A), $\log_{10}\left(\Delta\kappa^{-2}_{p_s(l)}+1\right)$ (B), $\log_{10}\left(\Delta\kappa^{-2}_{q_s(l)}+1\right)$ (C), and $\log_{10}\left(\Delta\kappa^{-2}_{p_i(0)}+1\right)$ (D) of the four observables to the quantum Fisher information $\log_{10}(F_\kappa+1)$ as functions of dimensionless lengths for parameters $\{\alpha = 10, \kappa = 0.5\}$, illustrating the sensitivity enhancement in the quadrature-PT phase unbroken region ($b = 0.2$).

to a tiny perturbation $\delta\kappa$ from a predefined κ-value. This system response is characterized by a susceptibility (SI), denoted as $\chi_\kappa^{q_i(0)}$, defined as $\partial\langle q_i(0)\rangle/\partial\kappa$, and derived from Equation 12. Next, the achievable accuracy of estimating the parameter κ's precision can be evaluated by considering the variance (3a) and susceptibility. This evaluation involves the relation $\Delta\kappa^2_{q_i(0)} = \langle\Delta q_i^2(0)\rangle/[\chi_\kappa^{q_i(0)}]^2$.

The inverse variance $\Delta\kappa^{-2}_{q_i(0)}$ determines the sensing power of the system, with its upper bound constrained by the QFI, F_κ. The QFI establishes the lower quantum Cramér-Rao bound, expressed as $F_\kappa \ngeq \Delta\kappa^{-2}_{q_i(0)}$, representing the utmost precision attainable through optimal measurement. For the seeding coherent input state $|\Phi\rangle_0$, the QFI of the system can be deduced from (see supplemental information for more detail),

$$F_\kappa = \left(\frac{d\mu}{d\kappa}\right)^\top V^{-1}\frac{d\mu}{d\kappa}. \qquad \text{(Equation 13)}$$

with $\top$ for a vector or matrix transpose. In Equation 13, the amplitude vector μ and V^{-1} are computed in the quadrature basis via $\mu_j = \langle\widehat{v}_j\rangle$ and $V_{j,k} = \frac{1}{2}\langle\widehat{v}_j\widehat{v}_k + \widehat{v}_k\widehat{v}_j\rangle - \langle\widehat{v}_j\rangle\langle\widehat{v}_k\rangle$, for $1 \le j, k \le 2$, with the column vector $\widehat{v} = (q_i(0), q_s(l), p_i(0), p_s(l))^\top$. As F_κ ascribes the entire system, it aligns with all other quantum observables. Notably, F_κ manifests differently in response to the contrasting PT domains. In supplemental information, we present logarithmic F_κ with distinctive characteristics in three circumstances: $b = 0.2$ (unbroken PT phase), $b = 1$ (EP), and $b = 2$ (breaking PT phase). Similarly, we can test κ-parameter estimation using the rest three single-mode quadratures (SI): $p_i(0), q_s(l)$, and $p_s(l)$. Our calculations indicate that our current scheme optimally supports quantum sensor performance in the quadrature-PT phase unbroken regime but away from the EP, distinguishing it from EP-based sensors. Numerical simulations in (Figure 4) demonstrate that the best sensing is achieved with a suitable medium length l, owing to the enlarged Hilbert space of the final system state. We illustrate four inverse variances before the quadrature-PT phase transitions in (Figures 4A–4D), portraying the ratios (insets) of $\Delta\kappa^{-2}_{q_i(0)}$, $\Delta\kappa^{-2}_{p_i(0)}$, $\Delta\kappa^{-2}_{q_s(l)}$, and $\Delta\kappa^{-2}_{p_s(l)}$ to F_κ, providing an instructive view of the data. Upon careful scrutiny of (Figure 4), we deduce that both $q_i(0)$ and $q_s(l)$ supply the maximum parameter estimation precision at the first oscillating peaks of $\log_{10}(\Delta\kappa^{-2}_{q_i(0)}+1)$ and $\log_{10}(\Delta\kappa^{-2}_{p_s(l)}+1)$ with respect to $\log_{10}(F_\kappa+1)$. However, overall, $q_s(l)$ outperforms $q_i(0)$ in sensing performance in terms of sensitivity and accuracy, entailing that the variance $\Delta\kappa^2_{q_s(l)}$ of passive quadrature-PT symmetry is smaller than the variance $\Delta\kappa^2_{q_i(0)}$ of active quadrature-PT. As l increases, the sensing ability of both observables worsens because F_κ gets larger, and the ratios become smaller. By contrast, $p_i(0)$ and $p_s(l)$ allow classical sensing exclusively with non-equivalent performance.

DISCUSSION

In contrast to previous studies, the type-II PSA-only twin-beam system serves as an optimal quantum platform for investigating dual opposing quadrature-PT symmetry. Our sophisticated theoretical framework allows for the exploration of profound C2Q transitions and establishes a unique link between PT symmetry, nonclassicality, and the EPR paradox. Our findings unveil nontrivial quantum aspects of PT symmetry beyond the capabilities of non-PSA-based systems, demonstrating promise for designing PT-enhanced quantum sensors that leverage anti-Hermiticity and squeezing. We anticipate that our proposed quadrature-PT scheme will unlock novel physical phenomena, enabling nonreciprocal transmission of continuous-variable (CV) qubits with minimal noise—crucial for CV-based quantum information processing and computing.[40] This capability poses a challenge for PIA-based apparatus.[4–17,25–27] By incorporating PSA, our system protects CVs from decoherence, compensating for loss through noiseless amplification and advancing CV-based quantum technologies. The nontrivial modulation and acceleration of quantum squeezing generation by PT symmetry further contribute to the development of diverse CV-based quantum technologies.

Limitations of the study

The results in this paper are based on purely theoretical derivations under ideal conditions and have not been experimentally conducted.

RESOURCE AVAILABILITY

Lead contact

Further information and requests for resources and samples should be directed to and will be fulfilled by the lead contact, Jianming Wen (jwen7@binghamton.edu).

Materials availability

This work did not generate new unique samples.

Data and code availability

- All data reported in this paper will be shared by the lead contact upon request.
- Code with instructions reported in this article will be shared by the lead contact upon request.
- Any additional information required to reanalyze the data reported in this paper is available from the lead contact upon request.

ACKNOWLEDGMENTS

We thank S.-W. Huang for enlightening discussions. This work was supported by NSF ExpandQISE-2329027. J.K., J.L., and Q.G. also acknowledge support from NSF ECCS-2240448. W.W. and D.L. were supported by the National Key R&D Program of China (2021YFA1400803), Guangdong Basic and Applied Basic Research Foundation (2022A1515140139), and Natural Science Foundation of China (62375089).

AUTHOR CONTRIBUTIONS

J.W. conceptualized the idea and oversaw the entire project, receiving critical support from D.L. and Q.G. W.W. conducted the theoretical calculations with assistance from J.K. and J.L., under the supervision of J.W. and D.L. All authors contributed to the discussions and writing of the manuscript.

DECLARATION OF INTERESTS

The authors declare no competing interests.

STAR★METHODS

Detailed methods are provided in the online version of this paper and include the following:

- KEY RESOURCES TABLE
- METHOD DETAILS
- QUANTIFICATION AND STATISTICAL ANALYSIS

SUPPLEMENTAL INFORMATION

Supplemental information can be found online at https://doi.org/10.1016/j.isci.2024.111655.

Received: August 27, 2024
Revised: October 22, 2024
Accepted: December 18, 2024
Published: December 25, 2024

REFERENCES

1. Bender, C.M., and Boettcher, S. (1998). Real spectra in non-Hermitian Hamiltonians having PT symmetry. Phys. Rev. Lett. *80*, 5243–5246.
2. Bender, C.M. (2007). Making sense of non-Hermitian Hamiltonians. Rep. Prog. Phys. *70*, 947–1018.
3. Mostafazadeh, A. (2010). Pseudo-Hermitian representation of quantum mechanics. Int. J. Geomet. Methods Mod. Phys. *07*, 1191–1306.
4. El-Ganainy, R., Makris, K.G., Christodoulides, D.N., and Musslimani, Z.H. (2007). Theory of coupled optical PT-symmetric structures. Opt. Lett. *32*, 2632–2634.
5. El-Ganainy, R., Makris, K.G., Khajavikhan, M., Musslimani, Z.H., Rotter, S., and Christodoulides, D.N. (2018). Non-Hermitian physics and PT symmetry. Nat. Phys. *14*, 11–19.
6. Özdemir, Ş.K., Rotter, S., Nori, F., and Yang, L. (2018). Parity-time symmetry and exceptional points in photonics. Nat. Mater. *18*, 783–798.
7. Wen, J., Jiang, X., Jiang, L., and Xiao, M. (2018). Parity-time symmetry in optical microcavity systems. J. Phys. B Atom. Mol. Opt. Phys. *51*, 222001.
8. Feng, L., El-Ganainy, R., and Ge, L. (2017). Non-Hermitian photonics based on parity-time symmetry. Nat. Photonics *11*, 752–762.
9. Konotop, V.V., Yang, J., and Zezyulin, D.A. (2016). Nonlinear waves in PT-symmetric systems. Rev. Mod. Phys. *88*, 035002.
10. Miri, M.-A., and Alù, A. (2019). Exceptional points in optics and photonics. Science *363*, eaar7709.
11. Longhi, S. (2018). Parity-time symmety meets photonics: A new twist in non-Hermitian optics. EPL *120*, 64001.
12. Zhang, Z., Ma, D., Sheng, J., Zhang, Y., Zhang, Y., and Xiao, M. (2018). Non-Hermitian optics in atomic systems. J. Phys. B Atom. Mol. Opt. Phys. *51*, 072001.
13. Suchkov, S.V., Sukhorukov, A.A., Huang, J., Dmitriev, S.V., Lee, C., and Kivshar, Y.S. (2016). Nonlinear Switching and solitons in PT-symmetric photonic systems. Laser Photon. Rev. *10*, 177–213.
14. Kottos, T., and Aceves, A.B. (2016). In Contemporary Optoelectronics, O. Shulika and I. Sukhoivanov, eds. (Springer).
15. Ashida, Y., Gong, Z., and Ueda, M. (2020). Non-Hermitian physics. Adv. Phys. X. *69*, 249–435.
16. Bergholtz, E.J., Budich, J.C., and Kunst, F.K. (2021). Exceptional toplogy of non-Hermitian systems. Rev. Mod. Phys. *93*, 015005.
17. Zyablovsky, A.A., Vinogradov, A.P., Pukkov, A.A., Dorofeenko, A.V., and Lisyansky, A.A. (2014). PT-symmetry in optics. Phys. Usp. *57*, 1063–1082.
18. Klauck, F., Teuber, L., Ornigotti, M., Heinrich, M., Scheel, S., and Szameit, A. (2019). Observation of PT-symmetric quantum interference. Nat. Photonics *13*, 883–887.
19. Naghiloo, M., Abbasi, M., Joglekar, Y.N., and Murch, K.W. (2019). Quantum state tomography across the exceptional point in a single dissipative qubit. Nat. Phys. *15*, 1232–1236.
20. Wu, Y., Liu, W., Geng, J., Song, X., Ye, X., Duan, C.-K., Rong, X., and Du, J. (2019). Observation of parity-time symmetry breaking in a single-spin system. Science *364*, 878–880.
21. Li, J., Harter, A.K., Liu, J., de Melo, L., Joglekar, Y.N., and Luo, L. (2019). Observation of parity-time symmetry breaking transitions in a dissipative Floquet system of ultracold atoms. Nat. Commun. *10*, 855.
22. Yu, S., Meng, Y., Tang, J.S., Xu, X.Y., Wang, Y.T., Yin, P., Ke, Z.J., Liu, W., Li, Z.P., Yang, Y.Z., et al. (2020). Experimental investigation of quantum PT-enhanced sensor. Phys. Rev. Lett. *125*, 240506.
23. Ding, L., Shi, K., Zhang, Q., Shen, D., Zhang, X., and Zhang, W. (2021). Experimental determination of PT-symmetric exceptional points in a single trapped ion. Phys. Rev. Lett. *126*, 083604.
24. Dogra, S., Melnikov, A.A., and Paraoanu, G.S. (2021). Quantum simulation of parity-time symmetry breaking with a superconducting quantum processor. Commun. Phys. *4*, 26.
25. Agarwal, G.S., and Qu, K. (2012). Spontaneous generation of photons in transmission of quantum fields in PT-symmetric optical systems. Phys. Rev. *85*, 031802.
26. Scheel, S., and Szameit, A. (2018). PT-symmetric photonic quantum systems with gain and loss do not exist. EPL *122*, 34001.

27. Lee, Y.-C., Hsieh, M.-H., Flammia, S.T., and Lee, R.-K. (2014). Local PT symmetry violates the no-signaling principle. Phys. Rev. Lett. *112*, 130404.

28. Wang, W., Zhai, Y., Liu, D., Jiang, X., Ghamsari, S.V., and Wen, J. (2024). Quadrature-PT symmetry: Classical-to-quantum transition in noise fluctuations. Preprint at arXiv. https://doi.org/10.48550/arXiv.2301.05511.

29. Han, P.-R., Wu, F., Huang, X.-J., Wu, H., Yang, Z.-B., Zou, C.-L., Yi, W., Zhang, M., Li, H., Xu, K., et al. (2022). PT symmetry and PT-enhanced quantum sensing in a spin-boson system. Preprint at arXiv. https://doi.org/10.1117/12.2657391.

30. Han, P.-R., Wu, F., Huang, X.-J., Wu, H.Z., Zou, C.-L., Yi, W., Zhang, M., Li, H., Xu, K., Zheng, D., et al. (2023). Exceptional entanglement phenomena: Non-Hermiticity meeting nonclassicality. Phys. Rev. Lett. *131*, 260201.

31. Reid, M.D. (1989). Demonstration of the Einstein-Podolsky-Rosen paradox using nondegereate parametric amplification. Phys. Rev. *40*, 913–923.

32. Reid, M.D., Drummond, P.D., Bowen, W.P., Cavalcanti, E.G., Lam, P.K., Bachor, H.A., Andersen, U.L., and Leuchs, G. (2009). The Einstein-Podolsky-Rosen paradox: From concepts to applications. Rev. Mod. Phys. *81*, 1727–1751.

33. Einstein, A., Podolsky, B., and Rosen, N. (1935). Can quantum-mechanical description of physical reality be considered complete? Phys. Rev. *47*, 777–780.

34. Vidal, G., and Werner, R.F. (2002). A computable measure of entanglement. Phys. Rev. *65*, 032314.

35. Plenio, M.B. (2005). The logarithmic negativity: A full entanglement monotone that is not convex. Phys. Rev. Lett. *95*, 090503.

36. Drummond, P.D., and Ficek, Z. (2004). Quantum Squeezing (Springer-Verlag).

37. Degen, C.L., Reinhard, F., and Cappellaro, P. (2017). Quantum sensing. Rev. Mod. Phys. *89*, 035002.

38. Luo, X.W., Zhang, C., and Du, S. (2022). Quantum squeezing and sensing with pseudo-anti-parity-time symmetry. Phys. Rev. Lett. *128*, 173602.

39. Niu, Z., Jiang, Y., Wen, J., Zhang, C., Du, S., and Novikova, I. (2024). Four-wave mixing with anti-parity-time symmetry in hot 85 Rb vapor. Appl. Phys. Lett. *124*, 044005.

40. Braunstein, S.L., and van Loock, P. (2005). Quantum information with continuous variables. Rev. Mod. Phys. *77*, 513–577.

STAR★METHODS

KEY RESOURCES TABLE

REAGENT or RESOURCE	SOURCE	IDENTIFIER
Software and algorithms		
Mathematica 12	Mathematica Software	https://www.wolfram.com/mathematica/
QUANTUM OPTICS	Scully, M. O. and Zubairy, M. S, 1997	https://books.google.com

METHOD DETAILS

Our article is a purely theoretical study. All equation derivation methods and details have been provided in the main text and supplementary materials.

QUANTIFICATION AND STATISTICAL ANALYSIS

There are no quantification or statistical analyses to include in this study.